BJP British Journal of Pharmacology

DOI:10.1111/bph.12609
www.brjpharmacol.org

RESEARCH PAPER

A physiologically based pharmacokinetic model of alvespimycin in mice and extrapolation to rats and humans

Zhe-Yi Hu[1], Jingtao Lu[2] and Yuansheng Zhao[2]

[1]*Department of Clinical Pharmacy, College of Pharmacy, University of Tennessee Health Science Center, Memphis, TN, USA, and* [2]*The Hamner Institutes for Health Sciences, Research Triangle Park, NC, USA*

Correspondence
Yuansheng Zhao, The Hamner Institutes for Health Sciences, 6 Davis Drive, Research Triangle Park, NC 27709, USA. E-mail: yuansheng.zhao@gmail.com

Keywords
PBPK modelling; alvespimycin; Hsp90 inhibitor; drug disposition; interspecies scaling

Received
22 May 2013
Revised
10 November 2013
Accepted
9 January 2014

BACKGROUND AND PURPOSE

Alvespimycin, a new generation of heat shock protein 90 (Hsp90) inhibitor in clinical trial, is a promising therapeutic agent for cancer. Pharmacokinetic models of alvespimycin would help in the understanding of drug disposition, predicting drug exposure and interpreting dose–response relationship. In the present study we aimed to develop a physiologically based pharmacokinetic (PBPK) model of alvespimycin in mice and evaluate the utility of the model for predicting alvespimycin disposition in other species.

EXPERIMENTAL APPROACH

A literature search was performed to collect pharmacokinetic data for alvespimycin. A PBPK model was initially constructed to demonstrate the disposition of alvespimycin in mice, and then extrapolated to rats and humans by taking into account the interspecies differences in physiological- and chemical-specific parameters.

KEY RESULTS

A PBPK model, employing a permeability-limited model structure and saturable tissue binding, was built in mice. It successfully characterized the time course of the disposition of alvespimycin in mice. After extrapolation to rats, the model simulated the alvespimycin concentration-time profiles in rat tissues with acceptable accuracies. Likewise, a reasonable match was found between the observed and simulated human plasma pharmacokinetics of alvespimycin.

CONCLUSIONS AND IMPLICATIONS

The PBPK model described here is beneficial to the understanding and prediction of the effects of alvespimycin in different species. It also provides a good basis for further development, which necessitates additional studies, especially those needed to clarify the in-depth mechanism of alvespimycin elimination. A refined PBPK model would benefit the understanding of dose–response relationships and optimization of dosing regimens.

Abbreviations

17-DMAG, 17-dimethylaminoethylamino-17-demethoxygeldanamycin; Hsp90, heat shock protein 90; PBPK, physiologically based pharmacokinetic(s)

Introduction

The ubiquitously expressed molecular chaperone heat shock protein 90 (Hsp90) plays an important role in the folding and conformation of many cellular signalling proteins, which are referred to as Hsp90 client proteins (Kamal *et al.*, 2003; Jhaveri *et al.*, 2012). Many of these client proteins, including Her-2, EGFR, Akt, Raf-1 and IKK, p53, v-Src, Bcr-Abl, Cdk4, Cdk6 and steroid receptors, are called oncoproteins because they are major components of cell signalling pathways that drive cellular proliferation and counteract apoptosis (Kamal *et al.*, 2003; Jhaveri *et al.*, 2012). The oncoproteins are frequently overexpressed and/or mutated in cancer, and contribute to cancer progression and therapy resistance (Beliakoff and Whitesell, 2004; Scaltriti *et al.*, 2012). It has been reported that the inhibition of Hsp90 is able to disrupt Hsp90's chaperone function, induce the proteasomal degradation of oncoproteins and ultimately produce antitumour effects (Whitesell and Lindquist, 2005; Workman and Powers, 2007; Trepel *et al.*, 2010). Therefore, Hsp90 inhibitors may represent a novel class of anticancer agents (Trepel *et al.*, 2010; Hong *et al.*, 2013).

The development of geldanamycin, the first Hsp90 inhibitor, as a drug candidate, was terminated because of serious hepatotoxicity. (Kim *et al.*, 2013). A geldanamycin analogue, 17-(allylamino)-17-demethoxygeldanamycin (tanespimycin, 17-AAG, NSC330507), is the first Hsp90 inhibitor entering clinical evaluation and has been undergoing phase II/III clinical investigations (Ramanathan *et al.*, 2010). However, tanespimycin also has a number of drawbacks (Glaze *et al.*, 2005). It is liable to be extensively metabolized to potentially toxic metabolites. Its poor aqueous solubility increases the complexity of its formulation preparation. The other geldanamycin derivative, 17-dimethylaminoethylamino-17-demethoxygeldanamycin (alvespimycin, 17-DMAG, KOS-1022, NSC707545), has shown more desirable pharmacokinetic and pharmacodynamic properties compared with tanespimycin, including increased metabolic stability, elevated water solubility, higher oral bioavailability, reduced hepatotoxicity and superior antitumour activity (Pacey *et al.*, 2011). Clinical studies have shown that alvespimycin has therapeutic effects and is well tolerated in patients with solid tumours, advanced solid tumours or acute myeloid leukaemia, indicating that it has potential to be a new drug of choice for cancer therapy (Kummar *et al.*, 2010; Lancet *et al.*, 2010; Ramanathan *et al.*, 2010; Pacey *et al.*, 2011; Jhaveri *et al.*, 2012).

Physiologically based pharmacokinetic (PBPK) modelling, treating the body as anatomical compartments connected by blood flow, utilizes physiological and chemical-specific parameters, as well as mathematic equations to quantitatively describe the *in vivo* disposition of xenobiotics (Barrett *et al.*, 2012). Compared with non-compartmental analysis and traditional compartmental modelling, which usually only focus on analysing concentration-time data in plasma, PBPK modelling is a more mechanistic approach for studying xenobiotic disposition (Nestorov, 2007). PBPK modelling is also capable of extrapolating across dose levels, formulations, routes of administration and species (Barrett *et al.*, 2012; Rostami-Hodjegan, 2012). Therefore, one application of PBPK models is predicting xenobiotic exposure in humans based on that in experimental animals. In addition, this type of model may allow for the evaluation of the effects of different factors including genetics, ages, diseases, drug–drug interactions, etc., on xenobiotic disposition. (Edginton *et al.*, 2008; Zhao *et al.*, 2011). Combined with pharmacodynamic data, PBPK modelling aids the understanding of therapeutic benefits and adverse effects of drugs, leading to optimized dosage regimens (Khalil and Laer, 2011). Because of these advantageous features, the interest in applying PBPK models in pharmaceutical industries and research academies has been rapidly growing in recent years (Rostami-Hodjegan, 2012).

Pharmacokinetic studies of alvespimycin have been conducted in mice, rats, dogs and humans (Egorin *et al.*, 2002; Eiseman *et al.*, 2005; Glaze *et al.*, 2005; Kummar *et al.*, 2010; Lancet *et al.*, 2010; Ramanathan *et al.*, 2010; Pacey *et al.*, 2011; Jhaveri *et al.*, 2012). However, it seemed valuable to develop a PBPK model for alvespimycin, which could provide further insight into the *in vivo* disposition of this drug candidate and have potential applications in the design of clinical studies. To our knowledge, no PBPK model of alvespimycin has been reported. Hence, in this study we developed a PBPK model for alvespimycin in mice. Extrapolation of this mouse PBPK model to rats and humans was also performed to examine the utility of the model for predicting the effects of alvespimycin exposure across species.

Methods

Data collection

'Alvespimycin', '17-DMAG', 'KOS-1022', 'NSC707545' and 'pharmacokinetics' were used as keywords in Pubmed to conduct a literature search. Publications containing pharmacokinetic data for alvespimycin in mice (Egorin *et al.*, 2002; Eiseman *et al.*, 2005), rats (Egorin *et al.*, 2002; Glaze *et al.*, 2005), dogs (Glaze *et al.*, 2005) and humans (Kummar *et al.*, 2010; Lancet *et al.*, 2010; Ramanathan *et al.*, 2010; Pacey *et al.*, 2011; Jhaveri *et al.*, 2012) were all retrieved.

Egorin and co-workers reported the concentration-time profiles of alvespimycin in multiple tissues, as well as the amount excreted into urine after i.v. dosing (75 $mg \cdot kg^{-1}$) to healthy female CD2F1 mice (Egorin *et al.*, 2002). Because their study provided the most informative data concerning alvespimycin disposition, it was used to develop the mouse PBPK model. Tissue distribution data for alvespimycin in mice bearing tumour xenografts (Eiseman *et al.*, 2005) were used to validate the mouse PBPK model. Alvespimycin concentration-time data in rat tissues (Egorin *et al.*, 2002), plasma pharmacokinetic profile in humans (Lancet *et al.*, 2010), as well as human plasma pharmacokinetic parameters (Kummar *et al.*, 2010; Ramanathan *et al.*, 2010; Pacey *et al.*, 2011; Jhaveri *et al.*, 2012), were used to assess interspecies extrapolation of the PBPK model. Other studies conducted in rats (Glaze *et al.*, 2005) and dogs (Glaze *et al.*, 2005) provided very limited pharmacokinetic data and thus were not included in our study. All data were directly extracted from tables or captured by digitization from figures.

PBPK modelling in mice

Based on the tissue distribution data available for alvespimycin in mice (Egorin *et al.*, 2002), the whole-body PBPK model

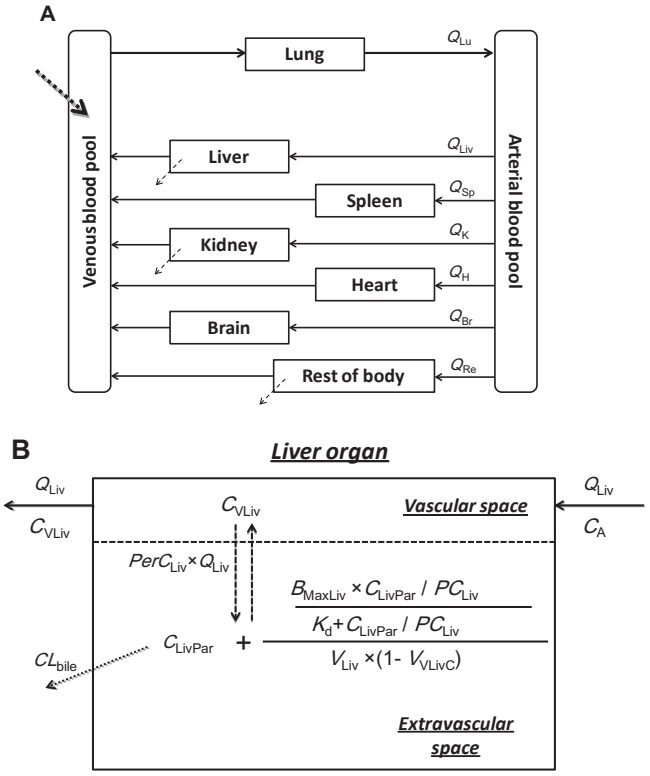

Figure 1

(A) Schematic representation of the whole-body PBPK model for alvespimycin. Q_{Lu}, Q_{Liv}, Q_{Sp}, Q_K, Q_H, Q_{Br} and Q_{Re} are blood flow to lung, liver, spleen, kidney, heart, brain and rest of the body compartment respectively. Dotted line represents dosing and dashed lines elimination. (B) Schematic representation of the model in the liver compartment for alvespimycin. Q_{Liv} is the blood flow rate to liver; V_{Liv} is the liver volume; V_{VLivC} is the fraction of vascular space in liver; C_A is the drug concentration in arterial blood pool; A_{VLiv} and C_{VLiv} are the drug amount and concentration in liver vascular space, respectively; A_{Liv} and C_{Liv} are the drug amount and concentration in liver extravascular space, respectively; PC_{Liv} is the liver to blood partition coefficient; $PerC_{Liv}$ is the relative permeability coefficient between vascular space and extravascular space in liver; C_{LivPar} is one portion of C_{Liv} and results from linear (non-saturable) binding to liver extravascular space; B_{MaxLiv} is the maximum capacity of non-linear (saturable) binding of alvespimycin to liver extravascular space; $B_{MaxLivC}$ is the maximum capacity of non-linear (saturable) binding of alvespimycin g^{-1} weight of liver extravascular space; K_d is the dissociation constant of non-linear (saturable) binding which was assumed identical among tissues to simply the model; and CL_{Bile} is the biliary clearance.

consisted of liver, kidney, heart, lung, brain, spleen, the rest of the body, arterial blood pool and venous blood pool (Figure 1A). All the compartments were connected by blood flow. Venous blood pool was regarded as the dosing site. Both renal (CL_{Urine}) and biliary (CL_{Bile}) elimination pathways, which were reported to be involved in the clearance of alvespimycin, were included. Urinary excretion of alvespimycin during 24 h post dosing accounted for 10.6–14.8% of delivered dose in mice (Egorin *et al.*, 2002). Because mouse biliary excretion data are not available, it was assumed to be the same as that in rats, that is ~2.32% of administered dose recovered in bile during 24 h post dosing (Egorin *et al.*, 2002). Elimination by metabolism was not included in the model structure because negligible metabolism of alvespimycin was reported in mice (Egorin *et al.*, 2002). As the sum of renal and biliary excretion accounts for less than 20% of the total dose, incorporation of an additional elimination pathway (CL_{Re}) was required to capture the concentration-time data in tissues. For simplicity, the additional clearance pathway was assigned to the rest of the body compartment (Figure 1A).

A permeability-limited model was used to describe the drug distribution into each tissue (Figure 1B, liver used as an example). Each tissue was divided into two subcompartments, that is vascular and extravascular space. PerC is the relative permeability coefficient, and the product of PerC and Q (tissue blood flow) represents the permeability clearance between vascular space and extravascular space. PC is the tissue to blood partition coefficient, which reflects the relative affinity of a chemical binding to tissue versus blood, assuming that the binding to both tissue and blood occurs in a linear and non-saturable manner (Kalvass *et al.*, 2007). Similar to the PBPK models of methotrexate (Bischoff *et al.*, 1971) and docetaxel (Bradshaw-Pierce *et al.*, 2007), a non-linear and saturable binding to tissue components, supposedly to Hsp90 proteins, was also included. Two parameters, B_{Max} (maximum binding capacity, unit as μg) and K_d (dissociation constant of binding, unit as $\mu g \cdot mL^{-1}$; a smaller K_d indicates higher binding affinity) were introduced to describe the non-linear and saturable binding process within tissue.

Because equations describing drug disposition in different tissue compartments are very similar, we only exhibited the equations for liver, arterial blood pool and venous blood pool.

Liver vascular space

$$\frac{dA_{VLiv}}{dt} = Q_{Liv} \times (C_A - C_{VLiv}) + PerC_{Liv} \times Q_{Liv} \times \left(\frac{C_{LivPar}}{PC_{Liv}} - C_{VLiv} \right) \quad (1)$$

$$C_{VLiv} = \frac{A_{VLiv}}{V_{Liv} \times V_{VLivC}} \quad (2)$$

Liver extravascular space

$$\frac{dA_{Liv}}{dt} = PerC_{Liv} \times Q_{Liv} \times \left(C_{VLiv} - \frac{C_{LivPar}}{PC_{Liv}} \right) - CL_{bile} \times \frac{C_{LivPar}}{PC_{Liv}} \quad (3)$$

$$C_{LivPar} = \frac{A_{Liv}}{V_{Liv} \times (1 - V_{VLivC}) + \frac{B_{MaxLiv}}{PC_{Liv} \times K_d + C_{LivPar}}} \quad (4)$$

$$A_{Liv} = C_{LivPar} \times V_{Liv} \times (1 - V_{VLivC}) + \frac{B_{MaxLiv} \times \frac{C_{LivPar}}{PC_{Liv}}}{K_d + \frac{C_{LivPar}}{PC_{Liv}}} \quad (5)$$

$$B_{MaxLiv} = B_{MaxLivC} \times V_{Liv} \times (1 - V_{VLivC}) \quad (6)$$

$$C_{Liv} = \frac{A_{Liv}}{V_{Liv} \times (1 - V_{VLivC})} \quad (7)$$

Where Q_{Liv} is the blood flow rate to liver; V_{Liv} is the liver volume; V_{VLivC} is the fraction of vascular space in liver; C_A is the drug concentration in arterial blood pool; A_{VLiv} and C_{VLiv} are the drug amount and concentration in liver vascular

space, respectively; A_{Liv} and C_{Liv} are the drug amount and concentration in liver extravascular space, respectively; PC_{Liv} is the liver to blood partition coefficient, $PerC_{Liv}$ is the relative permeability coefficient between vascular space and extravascular space in liver; C_{LivPar} is one portion of C_{Liv} and results from linear (non-saturable) binding to liver extravascular space; C_{LivPar} will be equal to C_{Liv} if there is no non-linear (saturable) binding, that is B_{MaxLiv} is 0; B_{MaxLiv} is the maximum capacity of non-linear (saturable) binding of alvespimycin to liver extravascular space, $B_{MaxLivC}$ is the maximum capacity of non-linear (saturable) binding of alvespimycin g^{-1} weight of liver extravascular space, K_d is the dissociation constant of non-linear (saturable) binding which was assumed to be identical among tissues to simplify the model; CL_{Bile} is the biliary clearance. Equation 1 describes the changing rate of alvespimycin amount in vascular space of liver; Equation 3 describes the changing rate of alvespimycin amount in extravascular space of liver; Equation 5 describes the alvespimycin amount in extravascular space of liver; Equation 4 is an algebraic equation and is deduced from Equation 5; Equation 6 describes B_{MaxLiv}.

Venous blood pool

$$C_{VM} = (Q_{Liv} \times C_{VLiv} + Q_K \times C_{VK} + Q_H \times C_{VH} + Q_{Br} \times C_{VBr} + Q_{Sp} \times C_{VSp} + Q_{Re} \times C_{VRe}) \times \frac{1}{Q_{Lu}} \quad (8)$$

$$\frac{dA_{VB}}{dt} = Q_{Lu} \times (C_{VM} - C_V) + Doserate \quad (9)$$

$$C_V = \frac{A_{VB}}{V_{VB}} \quad (10)$$

$$C_{Plasma} = \frac{C_V}{K_{BP}} \quad (11)$$

Where Q_K, Q_H, Q_{Br}, Q_{Sp}, Q_{Lu} and Q_{Re} are the blood flow rate to kidney, heart, brain, spleen, lung and the rest of the body, respectively; C_{VK}, C_{VH}, C_{VBr}, C_{VSp} and C_{VRe} are the alvespimycin concentration in the extravascular space of kidney, heart, brain, spleen and the rest of the body, respectively; C_{VM} is the input drug concentration to venous blood pool; V_{VB} is the volume of venous blood pool; C_V is the drug concentration in venous blood pool; C_{plasma} is the plasma concentration in venous blood pool; and K_{BP} is the blood to plasma concentration ratio. Dose rate is the alvespimycin dosing rate. Equation 9 describes the changing rate of alvespimycin amount in venous blood pool.

Arterial blood pool

$$\frac{dA_{AB}}{dt} = Q_{Lu} \times (C_{VLu} - C_A) \quad (12)$$

$$C_A = \frac{A_{AB}}{V_{AB}} \quad (13)$$

Where V_{AB} is the volume of arterial blood pool; A_{AB} is drug amount in arterial blood pool; and C_{VLu} is the drug concentration in lung vascular space. Equation 12 describes the changing rate of alvespimycin amount in arterial blood pool.

The mouse body weight was assumed to be 0.022 kg, and the cardiac blood flow was set as 13.98 mL·min^{-1} (Brown *et al.*, 1997). Other physiological parameters, such as blood flow to different organs, tissue volumes, fractions of vascular space in tissues, are listed in Table 1 (Davies and

Table 1

Physiological parameters for mouse, rat and human

	Blood flow (% of cardiac output)			Tissue volume (% of body weight)			Fraction of the vascular space		
Tissue	**Mouse**	**Rat**	**Human**	**Mouse**	**Rat**	**Human**	**Mouse**	**Rat**	**Human**
Lung	100	100	100	0.73	0.50	0.76	0.50	0.36	0.33[c]
Liver	2.0[a]	2.4[a]	6.0[a]	5.49	3.66	2.57	0.31	0.21	0.11
Kidney	9.1	14.1	19.0	1.67	0.73	0.44	0.24	0.16	0.36
Heart	6.6	4.9	4.0	0.50	0.33	0.47	0.17[d]	0.26	0.17[d]
Brain	3.3	2.0	12.0	1.65	0.57	2.00	0.03	0.03	0.04
Spleen	1.12[b]	0.85[b]	1.37[b]	0.35	0.20	0.26	0.17	0.22	0.30[e]
Blood	–	–	–	4.90	7.40	7.90	–	–	–
Rest of the body		[f]			[g]		0.04[h]	0.04[h]	0.01[h]

Except specified, all values are from Brown *et al.*, 1997. –, not applicable.
[a]Hepatic arterial blood flow.
[b]Values are from Davies *et al.*, 1993.
[c]Averaged value from mouse, rat and dog.
[d]Averaged value from rat and dog.
[e]Averaged value from mouse, rat and dog.
[f]100 subtract sum of blood flow of liver, kidney, heart, brain and spleen.
[g]Body weight subtract sum of weight of lung, liver, kidney, heart, brain and spleen.
[h]Values of muscle are used.

Table 2

Chemical-specific parameters in the alvespimycin PBPK model

Parameter	Notation	Units	Mouse	Rat	Human
Tissue/blood partition coefficient[a]					
Lung	PC_{Lu}	Unitless	1.29	1.29	1.29
Liver	PC_{Liv}	Unitless	2.42	2.42	2.42
Kidney	PC_{K}	Unitless	2.08	2.08	2.08
Heart	PC_{H}	Unitless	1.28	1.28	1.28
Brain	PC_{Br}	Unitless	0.147	0.147	0.147
Spleen	PC_{Sp}	Unitless	1.92	1.92	1.92
Rest of body	PC_{Re}	Unitless	1.20	1.20	1.20
Relative permeability coefficient[b]					
Lung	$PerC_{Lu}$	Unitless	0.01	0.003	0.003
Liver	$PerC_{Liv}$	Unitless	8.98	4.83	1.79
Kidney	$PerC_{K}$	Unitless	2.17	0.902	0.620
Heart	$PerC_{H}$	Unitless	9.44	8.20	9.301
Brain	$PerC_{Br}$	Unitless	0.008	0.008	0.001
Spleen	$PerC_{Sp}$	Unitless	0.072	0.061	0.035
Rest of body	$PerC_{Re}$	Unitless	0.58	0.384	0.467
Maximum capacity of alvespimycin saturable binding g^{-1} tissue[a]					
Liver	$B_{MaxLivC}$	$\mu g \cdot g^{-1}$ tissue	13.4	13.4	13.4
Kidney	B_{MaxKC}	$\mu g \cdot g^{-1}$ tissue	6.11	6.11	6.11
Spleen	B_{MaxSpC}	$\mu g \cdot g^{-1}$ tissue	8.93	8.93	8.93
Heart	B_{MaxHC}	$\mu g \cdot g^{-1}$ tissue	0.45	0.45	0.45
Lung	B_{MaxLuC}	$\mu g \cdot g^{-1}$ tissue	4.92	4.92	4.92
Brain	B_{MaxBrC}	$\mu g \cdot g^{-1}$ tissue	0.14	0.14	0.14
Rest of body	B_{MaxReC}	$\mu g \cdot g^{-1}$ tissue	0.01	0.01	0.01
Dissociation constant non-linear binding[a]	K_d	$\mu g \cdot mL^{-1}$	0.39	0.39	0.39
Biliary clearance[b]	CL_{Bile}	$mL \cdot min^{-1}$	0.025	0.13	5.56
Urinary clearance[b]	CL_{Urine}	$mL \cdot min^{-1}$	0.071	0.36	15.8
Additional clearance[b]	CL_{Re}	$mL \cdot min^{-1}$	0.402	2.05	89.3
Blood to plasma concentration ratio[c]	K_{BP}	Unitless	3	3	3

[a]Values in mouse model were estimated by fitting the model to the data and the same values were used in the rat and human model.
[b]Values in mouse model were estimated by fitting the model to the data. The values were then scaled for rat and human model.
[c]Value in mouse is estimated based on data in Egorin *et al.*, 2002 and the same value is used in rat and human model.

Morris, 1993; Brown *et al.*, 1997). A density of 1 was assumed for all tissues.

Coding of the PBPK model, as well as simulations were conducted in Berkeley Madonna™ (version 8.3.18; University of California, Berkeley, CA, USA). To estimate the chemical-specific parameters (PerC, PC, B_{Max}, K_d, CL), a simplified 'open loop' model (Nestorov, 2007; Pertinez *et al.*, 2013) with only one tissue compartment (as shown in Figure 1B), was developed. This 'open loop' model was used to estimate the chemical-specific parameters in a tissue-by-tissue manner. PerC, PC, B_{Max} and K_d for each tissue compartment were estimated, based on the concentration-time data in both tissue and plasma, as well as the fixed K_{BP} obtained from the literature. CL_{Bile} and CL_{Urine} were manually adjusted to match the cumulative biliary and urinary excretion respectively. The parameter values from the 'open loop' model were then used as initial estimates in the whole-body PBPK model (Figure 1A). Subsequently, all chemical-specific parameters including CL_{Re}, were fitted to match the observed tissue and plasma concentration-time profiles. The curve fitting algorithm in Berkeley Madonna is to minimize the root mean square (RMS) between predicted and experimental values. The goodness-of-fit was assessed by system convergence, least RMS and visual inspection. The final values for all chemical-specific parameters were summarized in Table 2.

Extrapolation of the mouse model to rats and humans

The mouse PBPK model was extrapolated to rats and humans, by taking into account the interspecies differences in

physiological and chemical-specific parameters. Mouse physiological parameters (organ volume, blood flow and fraction of vascular space in tissue) were replaced with corresponding values for rats or humans (Table 1). Body weights of 0.25 and 70 kg were assumed for rats and humans respectively. The cardiac blood flow of rats and humans were set as 110.4 and 5200 mL·min^{-1} respectively (Brown *et al.*, 1997).

PC, K_d and B_{MaxC} for the same type of tissue were assumed to be identical among the three species investigated. CL_{Bile}, CL_{Urine} and CL_{Re} for rats and humans were estimated using allometric equations (Sharma and McNeill, 2009; Hu and Hayton, 2001; Kagan *et al.*, 2011):

$$CL_{rat} = CL_{mouse} \times \left(\frac{BW_{rat}}{BW_{mouse}}\right)^{0.67} \quad (14)$$

$$CL_{human} = CL_{mouse} \times \left(\frac{BW_{human}}{BW_{mouse}}\right)^{0.67} \quad (15)$$

where CL_{mouse} denotes mouse CL_{Bile}, CL_{Urine} and CL_{Re}; CL_{rat} denotes rat CL_{Bile}, CL_{Urine} and CL_{Re}; CL_{human} denotes human CL_{Bile}, CL_{Urine} and CL_{Re}; BW_{mouse}, BW_{rat} and BW_{human} are body weights of mouse, rat and human, respectively; 0.67 is the allometric exponent.

Likewise, PerC values in each tissue of rats and humans were estimated using allometric equations:

$$PerC_{rat} \times Q_{rat} = PerC_{mouse} \times Q_{mouse} \times \left(\frac{BW_{rat}}{BW_{mouse}}\right)^{0.67} \quad (16)$$

$$PerC_{human} \times Q_{human} = PerC_{mouse} \times Q_{mouse} \times \left(\frac{BW_{human}}{BW_{mouse}}\right)^{0.67} \quad (17)$$

where $PerC_{mouse}$ and Q_{mouse} denote PerC and blood flow (Q) for each mouse tissue; $PerC_{rat}$ and Q_{rat} denote PerC and Q for each rat tissue; and $PerC_{human}$ and Q_{human} represent PerC and Q for each human tissue.

Human plasma pharmacokinetic parameters were calculated based on simulated time-concentration data in human plasma. The $AUC_{0\rightarrow infinity}$ was calculated in Berkeley Madonna as the integral of plasma drug concentration over time from zero to infinity. Infinity was treated as 10-fold of the time period of the reported plasma sample collection. C_{max} was obtained by extracting the highest one from the simulated drug concentration values. Because alvespimycin was injected i.v. in all clinical trials included in our study, total plasma clearance (CL_{plasma}) was calculated as dose divided by $AUC_{0\rightarrow infinity}$.

Results

Development of mouse PBPK model

A schematic representation of the whole-body PBPK model is shown in Figure 1A. Figure 1B depicts the detailed model structure for each tissue compartment. A permeability-limited model was utilized for each tissue compartment because the uptake of alvespimycin into tissues might not be instantaneous. The rate of drug distribution into tissues depends on tissue volume, tissue blood flow, tissue to blood partition coefficient, drug elimination within tissue, and the ability of the drug crossing tissue cell membranes and/or blood–tissue barriers such as blood–brain barrier (BBB) (Rowland and Tozer, 2005). Compounds with both polar surface area (PSA) < 90 Å^2 and molecular weight <450 Da can penetrate BBB readily (van de Waterbeemd and Gifford, 2003). Alvespimycin has a relatively large PSA (169 Å^2, calculated by http://www.molinspiration.com/cgi-bin/properties) and high molecular weight (616 Da), thus it is unlikely that alvespimycin can easily penetrate the BBB unless there are drug transporters assisting its transport into the brain. No study has demonstrated that alvespimycin is a substrate of any drug uptake transporter. Therefore, a permeability-limited model is appropriate for demonstrating the distribution of alvespimycin into the brain. The same assumptions may be applicable to other tissue compartments.

A prolonged and non-linear terminal phase was observed in the alvespimycin concentration-time profiles in tissues, especially in spleen, liver, kidney and lung (Figure 2). This characteristic was not adequately described by a permeability-limited model structure (data not shown). Considering alvespimycin is a selective and potent Hsp90 inhibitor, non-linear and saturable binding to tissue components, possibly to Hsp90 proteins, was added into the model scheme (Figure 1B). This modification not only improved model simulations, but also made the model more relevant to the biochemical process in the body. The K_d was ultimately estimated in our model to be 0.39 μg·mL^{-1} (~0.63 μM; Table 1). To our knowledge, there are no data concerning binding affinity of alvespimycin to mouse tissues available. Assuming that the binding affinity of alvespimycin to mouse tissues is comparable with that of its analogue tanespimycin (0.2–0.6 μM to mouse liver, kidney, brain, lung and heart tissue) (Kamal *et al.*, 2003), the estimated K_d value is reasonable.

Figure 2 shows the experimental concentration-time profiles of alvespimycin in mouse tissues (Egorin *et al.*, 2002), as well as the PBPK model simulations. For all tissues, model simulations closely mirrored the experimental concentration-time data. Because muscle constituted about half of the volume of rest of the body compartment (Brown *et al.*, 1997), drug concentrations in muscle were used to represent the concentrations in the rest of the body compartment.

The PBPK model, which was developed in healthy mice, was subsequently evaluated with time-concentration data from mice bearing tumour xenografts. The experimentally observed time-concentration profiles of alvespimycin in C.B-17 SCID mice bearing MDA-MB-231 human breast cancer xenografts (Eiseman *et al.*, 2005), were reasonably captured by our model (Supporting Information Figure S1).

Extrapolation of PBPK model to rats

Before extrapolation of this mice model to humans, we evaluated the performance of our PBPK model in predicting alvespimycin exposure in rats. Time-concentration profiles of alvespimycin in multiple rat tissues were collected from a previous publication (Egorin *et al.*, 2002), in which Fisher 344 rats were dosed with 10 mg·kg^{-1} alvespimycin, i.v. As shown in Figure 3, the model simulations acceptably approximated the observed time-concentration profiles in liver, kidney, heart, lung, spleen and rest of the body. However, the drug concentrations in the brain were significantly overestimated and those in plasma were also overestimated, to a lesser degree.

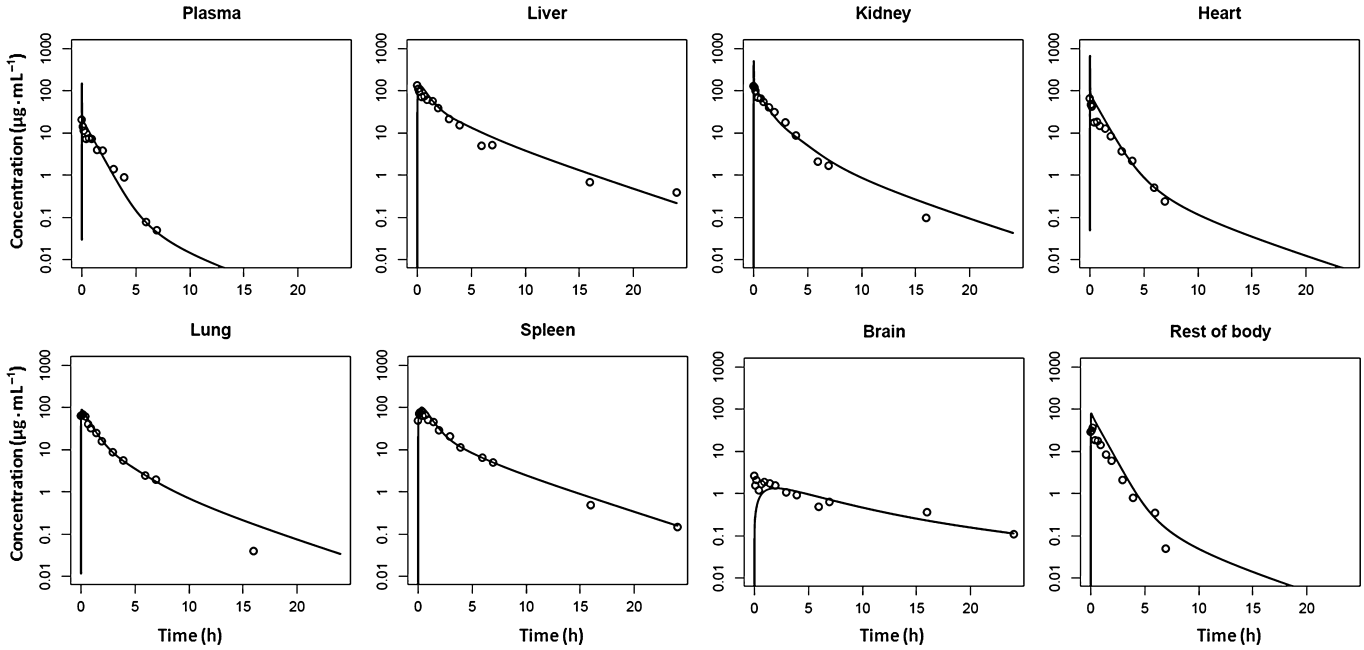

Figure 2

Observed and model-simulated alvespimycin time-concentration profiles in mouse tissues after i.v. dose at 75 mg·kg^{-1}. Blank circles represent observed data, solid lines represent simulation result.

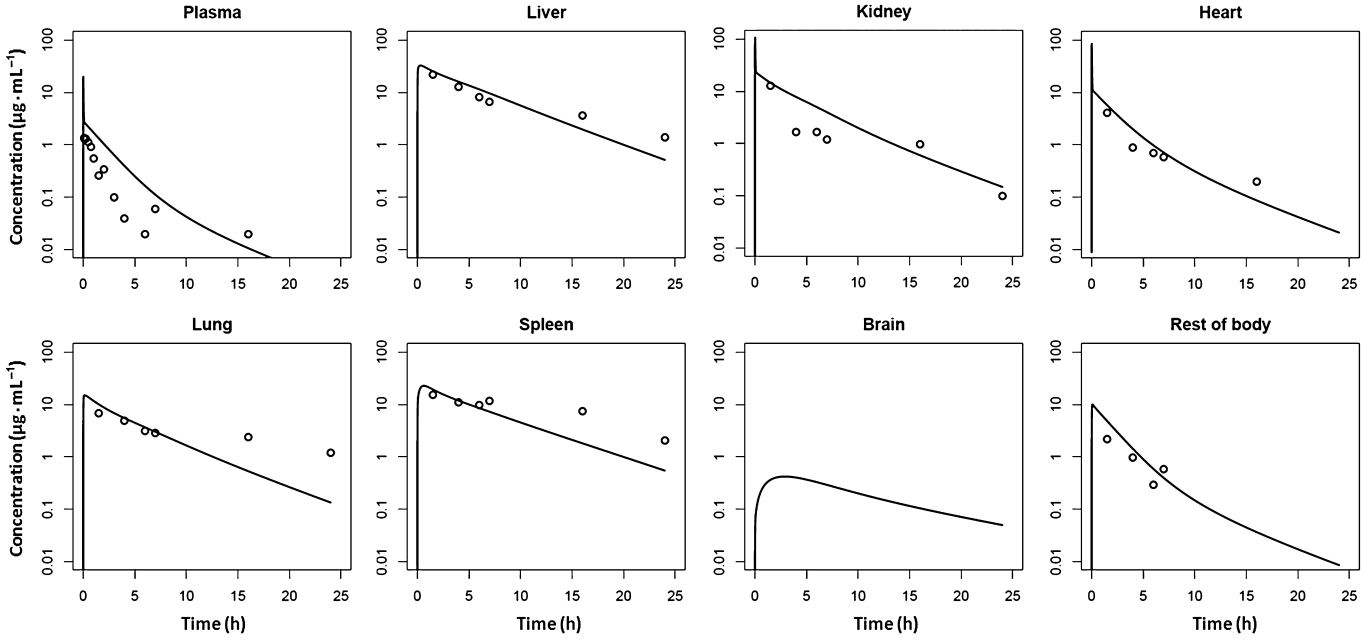

Figure 3

Observed and model-simulated alvespimycin time-concentration profiles in rat tissues after i.v. dose at 10 mg·kg^{-1}. Blank circles represent observed data, solid lines represent simulation result. The observed alvespimycin concentrations in rat brain were below the lower limit of quantification (Egorin *et al.*, 2002).

Extrapolation of PBPK model to humans

Among the literature reporting PK data of alvespimycin in humans, only one publication (Lancet *et al.*, 2010) provided plasma concentration-time profiles. In this study, human patients with acute myeloid leukaemia received 24 mg·m^{-2} alvespimycin by 1 h i.v. infusion. Using an averaged body weight of 70 kg and mean body surface area of 1.79 m^2 (Sacco *et al.*, 2010), the dose level of 24 mg·m^{-2} equates 0.614 mg·kg^{-1}. The plasma concentration-time profile in this study was used to assess the predictive performance of our PBPK model. Again, our model demonstrated an acceptable prediction of human plasma concentration-time profile of alvespimycin (Figure 4A), except that the experimental time-concentration profile had a little more curvature than the simulated one. Concentration-time profiles in human tissues were also simulated (Figure 4C and D). From high to low, alvespimycin exposure in tissues are ranked as follows: liver, kidney, spleen, lung, heart, rest of the body, plasma and brain.

To further evaluate the predictive performance of the human model, we simulated pharmacokinetic parameters ($AUC_{0\rightarrow infinity}$, C_{max} and CL_{plasma}) under different doses, and compared the predictions with the reported values in the literature. Observed and predicted pharmacokinetic parameter values are graphically presented in Figure 5 (exact values are summarized in Supporting Information Table S1).

Although there was considerable variations in the reported $AUC_{0\rightarrow infinity}$ values, a rough linear relationship between dose and $AUC_{0\rightarrow infinity}$ can be observed for experimental data and this was reasonably reflected by our simulations (Figure 5A). Similar conclusions can be made for observed and simulated C_{max} values (Figure 5B). Because of the large variations, experimental CL_{plasma} values did not appear to change with increasing doses. Simulated CL_{plasma} values were constant over the various doses and fell within the range of observed CL_{plasma} values (Figure 5C).

Discussion

Hsp90 has been considered as an attractive target in cancer therapy (Soti *et al.*, 2005; Banerji, 2009; Trepel *et al.*, 2010; Charlotte, 2013). The Hsp90 inhibitor, alvespimycin, has shown desirable pharmacokinetic and pharmacodynamic properties. However, alvespimycin has also been found to have toxic effects in several organs including the stomach, intestine, liver, spleen, etc., in preclinical studies in other species (Glaze *et al.*, 2005). Adverse events associated with alvespimycin in human patients were also observed (Kummar *et al.*, 2010; Lancet *et al.*, 2010; Ramanathan *et al.*, 2010; Pacey *et al.*, 2011; Jhaveri *et al.*, 2012). Hence, estimating the concentration-time profiles of alvespimycin in human

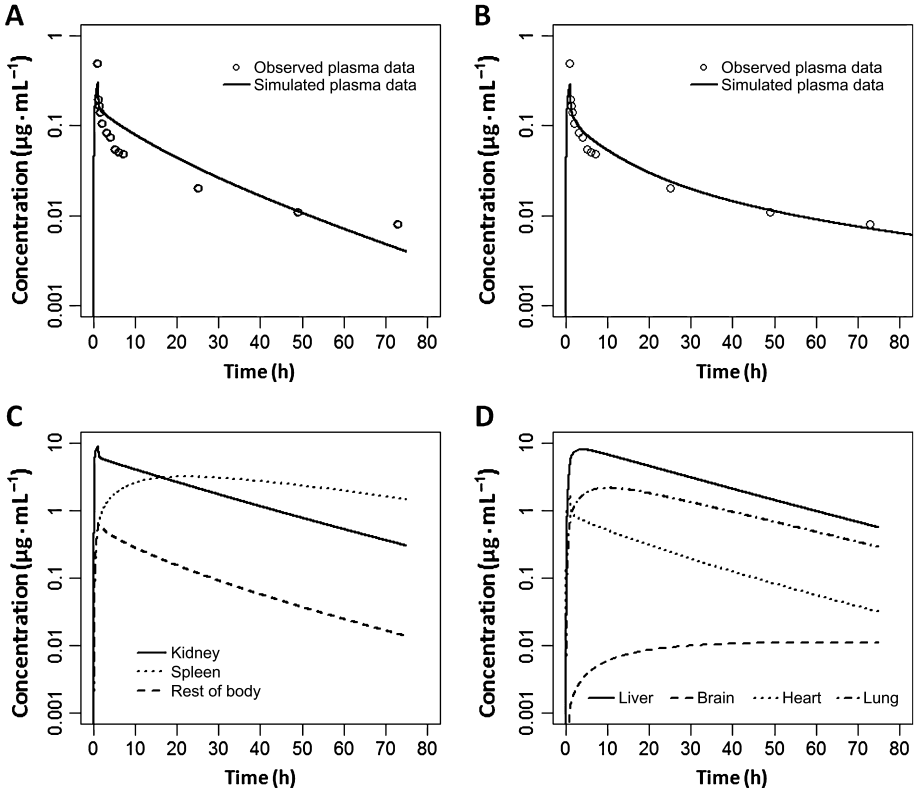

Figure 4

(A) Observed and model-simulated alvespimycin time-concentration profile in human plasma after an i.v. dose of 24 mg·m^{-2}, K_d = 0.39 μg·mL^{-1} in simulation. (B) Observed and model-simulated alvespimycin time-concentration profile in human plasma after an i.v. dose of 24 mg·m^{-2}, K_d = 0.05 μg·mL^{-1} in simulation. (C and D) Model simulated time-concentration profiles in human tissues, K_d = 0.39 μg·mL^{-1} in simulation.

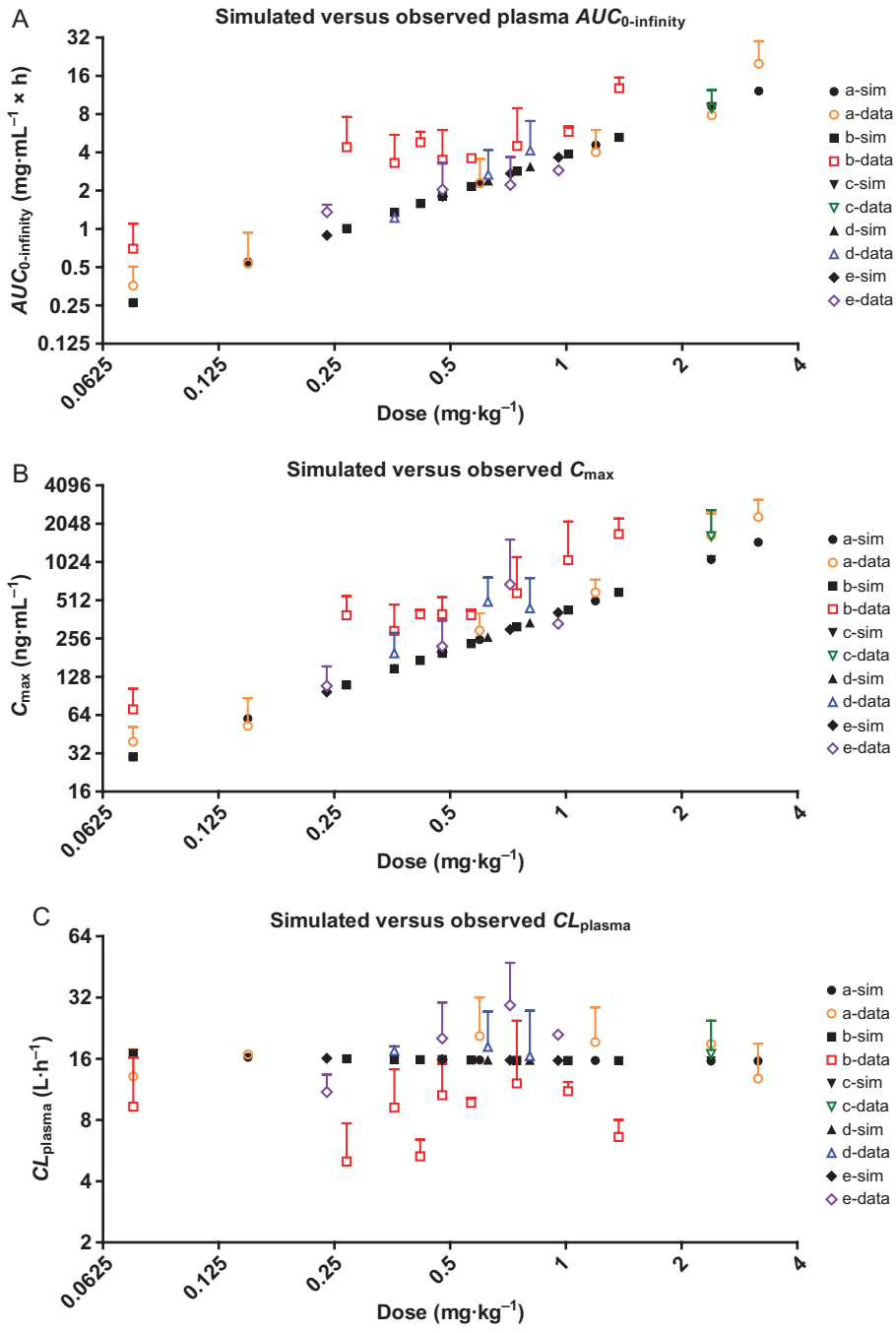

Figure 5

Pharmacokinetic parameters from reported human studies and from PBPK model simulations. (A) $AUC_{0\rightarrow infinity}$, (B) C_{max}, (C) CL_{plasma}. a-sim, simulated result based on dose level in Pacey *et al.*, 2011; a-data, reported data in Pacey *et al.*, 2011; b-sim, simulated result based on dose level in Ramanathan *et al.*, 2010; b-data, reported data in Ramanathan *et al.*, 2010; c-sim, simulated result based on dose level in Jhaveri *et al.*, 2012; c-data, reported data in Jhaveri *et al.*, 2012; d-sim, simulated result based on dose level in Kummar *et al.*, 2010; d-data, reported data in Kummar *et al.*, 2010; e-sim, simulated result based on dose level in Lancet *et al.*, 2010; e-data, reported data in Lancet *et al.*, 2010.

tissues, which is not readily achieved by experimental approaches, may aid the understanding of concentration–efficacy and concentration–toxicity relationship, leading to rational design of clinical dosing schedules. Our PBPK model would be of value in estimating alvespimycin exposure in human tissues because it acceptably predicted alvespimycin concentration-time profiles in human plasma, as well as human plasma pharmacokinetic parameters under different doses. The fact that our model reasonably reflected the time course of alvespimycin disposition in mouse and rat tissues,

improves the model's credibility in estimating alvespimycin exposure in human tissues.

A permeability-limited model structure was employed for each tissue compartment. The permeability clearance between vascular space and extravascular space, that is the product of PerC and tissue blood flow, is determined by PerC because of tissue blood flow being a constant under most circumstances. If PerC is high (for instance, >10), a permeability-limited model behaves like a perfusion-limited model, in which drug distribution from blood into tissue is instantaneous (Rowland and Tozer, 2005). Therefore, compared with a perfusion-limited model, the current model structure offers a wider range of application and more flexibility. Additionally, the fitted PerC values in some mouse tissues such as brain, lung and spleen (Table 1), were much smaller than 10, indicating that the movement of drug molecules between vascular space and extravascular space is a rate-limiting step in these tissues. Thus this observation confirmed our speculation that the dispersal of alvespimycin into tissues might not be instantaneous.

In rats, 12.5–16, ~2.32 and ~2.38% of the dose of alvespimysin injected were attributed to urinary excretion, biliary excretion and metabolism respectively (Egorin *et al.*, 2002). In mice, 10.6–14.8% of the dose delivered was recovered in urine and negligible metabolism was observed (Egorin *et al.*, 2002). Biliary excretion of alvespimysin in mice has not been reported and when developing the mouse PBPK model, it was assumed to be the same as that in rats. Both *in vivo* (Hwang *et al.*, 2006) and *in vitro* (Guo *et al.*, 2008; Zheng *et al.*, 2011) studies indicated that weak metabolism of alvespimysin occurs in humans. With regard to urinary and biliary excretion of alvespimysin in humans, no data are available so far. As the pattern of elimination for alvespimysin in humans is largely unknown, , in our current PBPK model, it was assumed to be similar to that in mice and rats. The hypothesis that a similar pattern of elimination for alvespimysin exists across species is also one of the rationales for interspecies extrapolation of this PBPK model.

The nature of the additional elimination pathway (CL_{Re}) needs to be elucidated. Intestinal excretion of alvespimysin from enterocytes to intestinal lumen might contribute to the additional clearance. Intestinal excretion is usually not a major route of drug elimination, but does play an important role in the elimination of those xenobiotics that have slow metabolism, or slow urinary or biliary excretion (McQueen, 2010). Coincidentally alvespimycin displayed weak elimination by metabolism, urinary and biliary excretion. The other possible explanation for the additional elimination pathway is that it represents binding of alvespimycin to cell membrane components, or trapping by cell organelles like lysosomes in tissues. Alvespimycin is a lipophilic weak base (Duvvuri *et al.*, 2006), which might be able to bind to acidic phospholipids such as phosphatidylserine. One study has shown that alvespimycin can be sequestrated in lysosomes (Ndolo *et al.*, 2010). It is possible that the bound or trapped alvespimycin molecules are released back to the plasma very slowly, leading to plasma concentrations under the detection limit of existing analytical methods. Under such conditions, the binding or trapping of alvespimycin in tissues behaves like an apparent clearance (Kagan *et al.*, 2011). Further studies are needed to elucidate the mechanism of this additional elimination pathway, which will deepen the understanding of alvespimycin pharmacokinetics and benefit the refinement of the current PBPK model.

In the extrapolation of the mouse PBPK model to rats and humans, some chemical-specific parameters, including PC, K_d and B_{MaxC} for the same type of tissue, remained unchanged. Other chemical-specific parameters (CL and PerC) were scaled with body weight using empirical allometric exponents. This manner of extrapolation for chemical-specific parameters is routinely used in PBPK modelling (Bischoff *et al.*, 1971; Anderton *et al.*, 2004; Meno-Tetang *et al.*, 2006; Bradshaw-Pierce *et al.*, 2007; Godin *et al.*, 2010; Kagan *et al.*, 2011; Hudachek and Gustafson, 2013), but may not always be accurate or valid because there are considerable differences in abundance and function of drug-metabolizing enzymes, drug transporters and other molecules across species (Hu and Hayton, 2001; Sharma and McNeill, 2009; Kenyon, 2012). All these confounding factors can contribute to the discrepancies between the simulated and observed data. In our study, most of the observed data were reasonably simulated by our PBPK model. However, rat brain concentrations were overestimated by model prediction (Figure 3), and the human plasma pharmacokinetic profile was not accurately predicted (Figure 4A). In the latter example, modification of the K_d value (from 0.39 to 0.05 $\mu g \cdot mL^{-1}$) in the human PBPK model enables an improved simulation (Figure 4A and B). This observation indicates that species-dependent affinity in the non-linear binding of alvespimycin to mouse and human tissue components may exist. Not taking into account these species-dependent differences could lead to imperfect interspecies extrapolation. Collectively, the discrepancies between simulations and the experimental data imply that once available, species-specific chemical-specific parameters should be incorporated to achieve better model prediction. Therefore, our PBPK model could be refined when more species-specific data and mechanisms regarding alvespimycin disposition become available.

Conclusion

In summary, a PBPK model was successfully developed to describe the time course of alvespimycin concentrations in plasma and seven tissues of mice. Saturable binding in tissues was employed to characterize the prolonged and non-linear terminal phase of concentration-time profiles in tissues. After extrapolating the mouse model to rats and humans, model simulations reasonably predicted alvespimycin concentration-time profiles in rat tissues and in human plasma, as well as human plasma pharmacokinetic parameters under different doses. Our model would be of value in understanding and predicting alvespimycin pharmacokinetics in different species. It also provided a good basis for further improvement, which necessitates additional studies, especially those to illuminate the entire mechanism of alvespimycin elimination. A refined PBPK model would have extensive potential applications, and ultimately benefit the optimization of dosing regimens to maximize therapeutic benefits while minimizing adverse effects of alvespimycin.

Conflict of interest

The authors declare no conflict of interest.

References

Anderton MJ, Manson MM, Verschoyle R, Gescher A, Steward WP, Williams ML *et al.* (2004). Physiological modeling of formulated and crystalline 3,3′-diindolylmethane pharmacokinetics following oral administration in mice. Drug Metab Dispos 32: 632–638.

Banerji U (2009). Heat shock protein 90 as a drug target: some like it hot. Clin Cancer Res 15: 9–14.

Barrett JS, Della Casa Alberighi O, Laer S, Meibohm B (2012). Physiologically based pharmacokinetic (PBPK) modeling in children. Clin Pharmacol Ther 92: 40–49.

Beliakoff J, Whitesell L (2004). Hsp90: an emerging target for breast cancer therapy. Anticancer Drugs 15: 651–662.

Bischoff KB, Dedrick RL, Zaharko DS, Longstreth JA (1971). Methotrexate pharmacokinetics. J Pharm Sci 60: 1128–1133.

Bradshaw-Pierce EL, Eckhardt SG, Gustafson DL (2007). A physiologically based pharmacokinetic model of docetaxel disposition: from mouse to man. Clin Cancer Res 13: 2768–2776.

Brown RP, Delp MD, Lindstedt SL, Rhomberg LR, Beliles RP (1997). Physiological parameter values for physiologically based pharmacokinetic models. Toxicol Ind Health 13: 407–484.

Charlotte H (2013). Lead identification: better HSP90 inhibitors. Nat Rev Drug Discov 12: 346.

Davies B, Morris T (1993). Physiological parameters in laboratory animals and humans. Pharm Res 10: 1093–1095.

Duvvuri M, Konkar S, Hong KH, Blagg BS, Krise JP (2006). A new approach for enhancing differential selectivity of drugs to cancer cells. ACS Chem Biol 1: 309–315.

Edginton AN, Theil FP, Schmitt W, Willmann S (2008). Whole body physiologically-based pharmacokinetic models: their use in clinical drug development. Expert Opin Drug Metab Toxicol 4: 1143–1152.

Egorin MJ, Lagattuta TF, Hamburger DR, Covey JM, White KD, Musser SM *et al.* (2002). Pharmacokinetics, tissue distribution, and metabolism of 17-(dimethylaminoethylamino)-17-demethoxygeldanamycin (NSC 707545) in CD2F1 mice and Fischer 344 rats. Cancer Chemother Pharmacol 49: 7–19.

Eiseman JL, Lan J, Lagattuta TF, Hamburger DR, Joseph E, Covey JM *et al.* (2005). Pharmacokinetics and pharmacodynamics of 17-demethoxy 17-[[(2-dimethylamino)ethyl]amino] geldanamycin (17DMAG, NSC 707545) in C.B-17 SCID mice bearing MDA-MB-231 human breast cancer xenografts. Cancer Chemother Pharmacol 55: 21–32.

Glaze ER, Lambert AL, Smith AC, Page JG, Johnson WD, McCormick DL *et al.* (2005). Preclinical toxicity of a geldanamycin analog, 17-(dimethylaminoethylamino)-17-demethoxygeldanamycin (17-DMAG), in rats and dogs: potential clinical relevance. Cancer Chemother Pharmacol 56: 637–647.

Godin SJ, DeVito MJ, Hughes MF, Ross DG, Scollon EJ, Starr JM *et al.* (2010). Physiologically based pharmacokinetic modeling of deltamethrin: development of a rat and human diffusion-limited model. Toxicol Sci 115: 330–343.

Guo W, Reigan P, Siegel D, Ross D (2008). Enzymatic reduction and glutathione conjugation of benzoquinone ansamycin heat shock protein 90 inhibitors: relevance for toxicity and mechanism of action. Drug Metab Dispos 36: 2050–2057.

Hong DS, Banerji U, Tavana B, George GC, Aaron J, Kurzrock R (2013). Targeting the molecular chaperone heat shock protein 90 (HSP90): lessons learned and future directions. Cancer Treat Rev 39: 375–387.

Hu TM, Hayton WL (2001). Allometric scaling of xenobiotic clearance: uncertainty versus universality. AAPS PharmSci 3: E29.

Hudachek SF, Gustafson DL (2013). Physiologically based pharmacokinetic model of lapatinib developed in mice and scaled to humans. J Pharmacokinet Pharmacodyn 40: 157–176.

Hwang K, Scripture CD, Gutierrez M, Kummar S, Figg WD, Sparreboom A (2006). Determination of the heat shock protein 90 inhibitor 17-dimethylaminoethylamino-17-demethoxygeldanamycin in plasma by liquid chromatography-electrospray mass spectrometry. J Chromatogr B Analyt Technol Biomed Life Sci 830: 35–40.

Jhaveri K, Miller K, Rosen L, Schneider B, Chap L, Hannah A *et al.* (2012). A phase I dose-escalation trial of trastuzumab and alvespimycin hydrochloride (KOS-1022; 17 DMAG) in the treatment of advanced solid tumors. Clin Cancer Res 18: 5090–5098.

Kagan L, Gershkovich P, Wasan KM, Mager DE (2011). Physiologically based pharmacokinetic model of amphotericin B disposition in rats following administration of deoxycholate formulation (Fungizone(R)): pooled analysis of published data. AAPS J 13: 255–264.

Kalvass JC, Maurer TS, Pollack GM (2007). Use of plasma and brain unbound fractions to assess the extent of brain distribution of 34 drugs: comparison of unbound concentration ratios to *in vivo* p-glycoprotein efflux ratios. Drug Metab Dispos 35: 660–666.

Kamal A, Thao L, Sensintaffar J, Zhang L, Boehm MF, Fritz LC *et al.* (2003). A high-affinity conformation of Hsp90 confers tumour selectivity on Hsp90 inhibitors. Nature 425: 407–410.

Kenyon EM (2012). Interspecies extrapolation. Methods Mol Biol 929: 501–520.

Khalil F, Laer S (2011). Physiologically based pharmacokinetic modeling: methodology, applications, and limitations with a focus on its role in pediatric drug development. J Biomed Biotechnol 2011: 907461.

Kim T, Keum G, Pae AN (2013). Discovery and development of heat shock protein 90 inhibitors as anticancer agents: a review of patented potent geldanamycin derivatives. Expert Opin Ther Pat 23: 919–943.

Kummar S, Gutierrez ME, Gardner ER, Chen X, Figg WD, Zajac-Kaye M *et al.* (2010). Phase I trial of 17-dimethylaminoethylamino-17-demethoxygeldanamycin (17-DMAG), a heat shock protein inhibitor, administered twice weekly in patients with advanced malignancies. Eur J Cancer 46: 340–347.

Lancet JE, Gojo I, Burton M, Quinn M, Tighe SM, Kersey K *et al.* (2010). Phase I study of the heat shock protein 90 inhibitor alvespimycin (KOS-1022, 17-DMAG) administered intravenously twice weekly to patients with acute myeloid leukemia. Leukemia 24: 699–705.

McQueen CA (2010) Comprehensive Toxicology. Elsevier: Amsterdam.

Meno-Tetang GM, Li H, Mis S, Pyszczynski N, Heining P, Lowe P *et al.* (2006). Physiologically based pharmacokinetic modeling of FTY720 (2-amino-2[2-(-4-octylphenyl)ethyl]propane-1,3-diol hydrochloride) in rats after oral and intravenous doses. Drug Metab Dispos 34: 1480–1487.

Ndolo RA, Forrest ML, Krise JP (2010). The role of lysosomes in limiting drug toxicity in mice. J Pharmacol Exp Ther 333: 120–128.

Nestorov I (2007). Whole-body physiologically based pharmacokinetic models. Expert Opin Drug Metab Toxicol 3: 235–249.

Pacey S, Wilson RH, Walton M, Eatock MM, Hardcastle A, Zetterlund A *et al.* (2011). A phase I study of the heat shock protein 90 inhibitor alvespimycin (17-DMAG) given intravenously to patients with advanced solid tumors. Clin Cancer Res 17: 1561–1570.

Pertinez H, Chenel M, Aarons L (2013). A physiologically based pharmacokinetic model for strontium exposure in rat. Pharm Res 30: 1536–1552.

Ramanathan RK, Egorin MJ, Erlichman C, Remick SC, Ramalingam SS, Naret C *et al.* (2010). Phase I pharmacokinetic and pharmacodynamic study of 17-dimethylaminoethylamino-17-demethoxygeldanamycin, an inhibitor of heat-shock protein 90, in patients with advanced solid tumors. J Clin Oncol 28: 1520–1526.

Rostami-Hodjegan A (2012). Physiologically based pharmacokinetics joined with *in vitro–in vivo* extrapolation of ADME: a marriage under the arch of systems pharmacology. Clin Pharmacol Ther 92: 50–61.

Rowland M, Tozer TN (2005) Clinical Pharmacokinetics/ Pharmacodynamics. Lippincott Williams and Wilkins: Philadelphia.

Sacco JJ, Botten J, Macbeth F, Bagust A, Clark P (2010). The average body surface area of adult cancer patients in the UK: a multicentre retrospective study. PLoS ONE 5: e8933.

Scaltriti M, Dawood S, Cortes J (2012). Molecular pathways: targeting hsp90 – who benefits and who does not. Clin Cancer Res 18: 4508–4513.

Sharma V, McNeill JH (2009). To scale or not to scale: the principles of dose extrapolation. Br J Pharmacol 157: 907–921.

Soti C, Nagy E, Giricz Z, Vigh L, Csermely P, Ferdinandy P (2005). Heat shock proteins as emerging therapeutic targets. Br J Pharmacol 146: 769–780.

Trepel J, Mollapour M, Giaccone G, Neckers L (2010). Targeting the dynamic HSP90 complex in cancer. Nat Rev Cancer 10: 537–549.

van de Waterbeemd H, Gifford E (2003). ADMET *in silico* modelling: towards prediction paradise? Nat Rev Drug Discov 2: 192–204.

Whitesell L, Lindquist SL (2005). HSP90 and the chaperoning of cancer. Nat Rev Cancer 5: 761–772.

Workman P, Powers MV (2007). Chaperoning cell death: a critical dual role for Hsp90 in small-cell lung cancer. Nat Chem Biol 3: 455–457.

Zhao P, Zhang L, Grillo JA, Liu Q, Bullock JM, Moon YJ *et al.* (2011). Applications of physiologically based pharmacokinetic (PBPK) modeling and simulation during regulatory review. Clin Pharmacol Ther 89: 259–267.

Zheng N, Zou P, Wang S, Sun D (2011). *In vitro* metabolism of 17-(dimethylaminoethylamino)-17-demethoxygeldanamycin in human liver microsomes. Drug Metab Dispos 39: 627–635.

Supporting information

Additional Supporting Information may be found in the online version of this article at the publisher's web-site:

http://dx.doi.org/10.1111/bph.12609

Figure S1 Observed and model-simulated alvespimycin time-concentration profiles in tissues of mice bearing MDA-MB-231 human breast cancer xenografts after an i.v. dose of 75 mg·kg^{-1}. Blank circles represent observed data, solid lines represent simulation result.

Table S1 Observed and model-simulated pharmacokinetic parameters in human plasma